

Tunable Nanostructure of TiO₂/Reduced Graphene Oxide Composite for High Photocatalysis

Di He, Yongli Li*, Jinshu Wang*, Yilong Yang, Qier An

Key Laboratory of Advanced Functional Materials, Ministry of Education, School of Materials Science and Engineering, Beijing University of Technology, Beijing 100124, China

*Correspondence to:

Li Y,
Tel: +86-10-67391101
Fax: +86-10-67391101
E-mail: lyi@bjut.edu.cn

Wang J,
Tel: +86-10-67392668
Fax: +86-10-67391101
E-mail: wangjsh@bjut.edu.cn

Received December 11, 2015

Revised January 23, 2016

Accepted January 25, 2016

In this study TiO₂/reduced graphene oxide (TiO₂/rGO) bipyramid with tunable nanostructure was fabricated by two-step solvothermal process and subsequent heat-treatment in air. The as-synthesized anatase TiO₂ nanocrystals possessed morphological bipyramid with exposed dominantly by (101) facets. Polyethylenimine was utilized during the combination of TiO₂ and graphene oxide (GO) to tune the surface charge, hindering the restack of graphene during solvothermal process and resulting in 1 to 5 layers of rGO wrapped on TiO₂ surface. After a further calcination, a portion of carbon quantum dots (CQDs) with a diameter about 2 nm were produced owing to the oxidizing and cutting of rGO on TiO₂. The as-prepared TiO₂/rGO hybrid showed a highly photocatalytic activity, which is about 3.2 and 7.7 times enhancement for photodegradation of methyl orange with compared to pure TiO₂ and P25, respectively. We assume that the improvement of photocatalysis is attributed to the chemical bonding between rGO/CQDs and TiO₂ that accelerates photogenerated electron-hole pair separation, as well as enhances light harvest.

Key Words: TiO₂, Graphene wrapping, Carbon quantum dots, Photodegradation

INTRODUCTION

Among many intensive studied semiconductor photocatalysis, TiO₂ is still the most promising candidate for its strong oxidative power, high chemical and photocatalytic stability, abundant storage, low cost and environment friendly (Cargnello et al., 2014; Fattakhova-Rohlfing et al., 2014; Wang & Sasaki, 2014). But two major limits confine its wide application, *ca.* large band gap (about 3.2 eV for anatase) and high recombination rate of electron-hole pairs, resulting in that it is only sensitive to light below 387 nm in ultraviolet (UV) range and relatively lower photocatalytic performance since the photocatalytic activity is strongly dependent on the separation of photogenerated carriers (Chen et al., 2012; Wang et al., 2014). Numerous efforts, such as doping, have been used to handle these problems, which could tune conduction band and/or valence band to shorten band gap

but it faces weak redox ability or thermal instability. Coupling TiO₂ with other conductor is an effective way to facilitate charge separation. Graphene, as a two-dimensional sp² carbon network arranged in a honeycomb structure, is one of the hottest materials in recent years owing to its unique electronic, optical, mechanical and catalytic properties (Cao et al., 2010; Li et al., 2011, 2013; Wang et al., 2009). Graphene-contained composite materials may exhibit enhanced photocatalytic activity due to the excellent conductivity (5,000 Wm⁻¹ K⁻¹) allowing an excellent mobility of excited-state electrons and hindering electron-hole recombination, high theoretical specific surface area (2,600 m² g⁻¹) which can provide more active sites and intense light absorption extend to visible light region (Allen et al., 2009). Zhang et al. (2014) fabricated TiO₂ nanotube (NT) modified by graphene showed a photocurrent density of 1.44 mA cm⁻² at 1.23 V vs. reversible hydrogen electrode, which is notably increased by ~140% compared

This work was supported by the National Natural Science Foundation (51471006), National Outstanding Young Investigator Grant of China (51225402) and Beijing Natural Science Foundation (2151001).

© This is an open-access article distributed under the terms of the Creative Commons Attribution Non-Commercial License (<http://creativecommons.org/licenses/by-nc/4.0>) which permits unrestricted noncommercial use, distribution, and reproduction in any medium, provided the original work is properly cited.
Copyrights © 2016 by Korean Society of Microscopy

to the bare TiO₂ NTs under standard reporting conditions. Zhang et al. (2009) fabricated P25-graphene composite which showed higher photodegradation rate than pure P25 for both UV and visible light conditions.

It is well known that Fermi levels of TiO₂ and graphene are different which allow the charge transfer from TiO₂ to graphene and extend light absorption to visible light region when they contact. However, graphene-based composites usually show the particles-on-a-sheet geometry, which is of point-to-surface contact. Kim et al. (2012) prepared a nanosized graphene oxide (GO)-coated TiO₂ core/shell structure by a two-step oxidation process, indicating a surface-to-surface contact between reduced graphene oxide (rGO) and TiO₂, which exhibited better interfacial electron transfer. In this study, we adopt a solvothermal-calcination approach to reduce GO and fabricate core-shell type of TiO₂/rGO composite. By the use of electrostatic interactions between TiO₂ and GO owing to its surface charge difference, we adopt polyethylenimine (PEI) as the surface charge modulator to combine TiO₂ and graphene and to form flocculation. As a result, the TiO₂ particles are uniformly distributed on graphene sheets, resulting in 1 to 5 layers of graphene sheets entirely wrapped on TiO₂ surface. After a heat treatment in air, some carbon quantum dots (CQDs) are produced from the decomposition of graphene. Compared to pure TiO₂, TiO₂/rGO composite exhibits higher photocatalytic activity caused by the intimate contact between TiO₂ and rGO/CQDs.

MATERIALS AND METHODS

Chemicals and Materials

N, N-dimethylformamide (DMF, ≥99.5%) and acetic acid (HAc, ≥99.5%) were purchased from Beijing Chemical Works (China), respectively. Titanium (IV) n-butoxide (TBOT, ≥99%) and PEI (99%) were purchased from Alfa Aesar (China), Graphene oxide was purchased from Nanjing XFNANO Tech. Co. (China). All chemicals were used as received without further purification.

Methods

Preparation of TiO₂

Anatase TiO₂ bipyrnid nanoparticles were prepared by solvothermal process according to the previous report (Wu et al., 2012). In a typical synthesis procedure, 6 mL of DMF and 4 mL of HAc were thoroughly stirred for 30 minutes, then 2 mL of TBOT were added drop by drop, after stirring for 1 hour the solution was transferred into a Teflon-lined stainless steel autoclave and kept at 200°C for 24 hours. After cooling to the room temperature, the product was collected and washed with ethanol for several times, thoroughly dried in an oven at 60°C and finally heated at 350°C for 2 hours in air.

Synthesis of TiO₂/rGO

One hundred milligram of the as-prepared TiO₂ was added into 400 mL water and stirred for 30 minutes, 2 mL (1 mg/mL) GO was dropped into TiO₂ aqueous suspension, then 0.6 mL PEI (0.2 mg/mL) was added and stirred overnight. The mixed solution was centrifuged, the collected sample was dispersed with 10 mL ethanol and transferred into a Teflon-lined stainless steel autoclave and then kept at 130°C for 24 hours which is denoted as TiO₂/rGO. Finally, the TiO₂/rGO was collected and washed thoroughly with ethanol for three times, dried in an oven at 60°C overnight and heated in muffle furnace at 320°C for 8 hours, denoted as TiO₂/rGO-320.

Characterizations

The composites were characterized using a X-ray diffraction (Shimadzu XRD-7000, operating at 40 kV, 40 mA for Cu K α radiation, $\lambda=0.15418$ nm; Shimadzu, Japan). Transmission electron microscopy (TEM) and high-resolution TEM (HRTEM) characterizations were performed with a JEM-2010 (JEOL, Japan) operated at 200 kV. Nitrogen adsorption-desorption isotherm measurements were conducted at 77 K using an ASAP 2020 (Micromeritics Instrument, USA). Before analysis, all samples were pretreated by degassing at 150°C for 8 hours to remove any adsorbed species. UV-Vis absorption spectra were recorded with a Shimadzu-3600 Plus UV-Vis spectrophotometer (Shimadzu) using BaSO₄ as the background. X-ray photoelectron spectra (XPS) of the samples were measured using a PHI 5300 ESCA system (PerkinElmer, USA) with an Al K X-ray photoelectron spectrometer at 150 W. Fourier transform infrared (FTIR) spectroscopy (Frontier; PerkinElmer) with a resolution of 1 cm⁻¹ between 4,000 and 450 cm⁻¹ at room temperature under air atmosphere.

Photocatalytic Activity Test

Photocatalytic activity was evaluated by measuring the degradation rate of methyl orange (MO) in aqueous solution under UV light irradiation. The reaction solution contained 50 mg photocatalyst mixed with 50 mL aqueous solution of 10 mg/L MO in an 80 mL cylindrical quartz photochemical reactor with water circulation facility. The pH value of the above solution was adjusted to 2.9 to 3.0 using H₂SO₄ solution to ensure its characteristic wavelength max unchanged during measurement. The photocatalytic test was conducted by low intensity irradiation with light emitting diode lamps (3 W×4,370~375 nm, about 1.5 mW/cm²), which was located at 5 cm away from the surface of reaction solution. The concentration of MO during the degradation was tested using a UV-Vis spectrometer. Prior to irradiation, the suspension was continuously stirred in darkness for 1 hour to ensure the achievement of an adsorption-desorption equilibrium. At a given time interval (30 seconds), 2 mL suspension were

sampled and separated through centrifugation at 10,000 rpm. The supernatants were extracted to examine the degradation of MO at 501 nm on a UV-Vis spectrophotometer.

RESULTS AND DISCUSSION

Morphology and Structure Characterization

X-ray diffraction measurements were performed to investigate the crystalline structure and phase composition information, as shown in Fig. 1. Both pure TiO₂ and TiO₂/rGO-320 exhibited typical diffraction peaks of anatase phase (tetragonal, *I*_{41/amd}, JCPDS, No. 21-1272) (Yang et al., 2009) with high crystallinity. This result demonstrates that the solvothermal and heat process did not have obvious impact on TiO₂ phase. A peak starts from 24.3° and overlap with (101) peak of anatase, indicating the reduction of GO to rGO. However, the peak intensity is weak due to the low percentage of GO in the total composite (2 wt%) (Li et al., 2013; Tang et al., 2010; Zou et al., 2015). No peak shift is detected, indirectly demonstrating that rGO only exist on TiO₂ surface without doping into TiO₂ lattice.

Fig. 2A and B show the scanning electron microscopy images of TiO₂/rGO and TiO₂/rGO-320. Both TiO₂/rGO and TiO₂/rGO-320 have the same bipyramid-shape, similar to pure anatase TiO₂ (Fig. 2C), indicating that the heat treatments did not have impact on morphology. Interestingly, no obvious rGO sheets were found, even though we changed randomly to different locations, suggesting partially altered structure of particles-on-a-sheet geometry. This is consistent with TEM observations (Fig. 2C and D). Fig. 2C and the insert selected area electron diffraction pattern show a single-crystal structure with an interfacial angle ~68.3° of two adjacent faces which is the same as the theoretical value for the angle

between the (001) and (101) planes of anatase (Liu et al., 2015; Yang et al., 2008). The TiO₂ in TiO₂/rGO shows high exposure of (101) facets as shown in the HRTEM images (Fig. 2E). Notedly, most TiO₂ is wrapped by 1 to 5 layers of graphene sheets and form heterojunction interface. Due to the assistance of PEI, it ensures an intense contact between TiO₂ and GO and prevents GO from aggregation. Additionally, after a calcination procedure in air, as shown in Fig. 2F, some CQDs (about 2 nm in diameter) were produced. We assume these CQDs come from the cutting of rGO during the heat process and are fixed on TiO₂.

Fig. 3 shows the nitrogen adsorption-desorption isotherm and pore size distribution curve (inset), the physical properties are summarized in Table 1. All the tested pure TiO₂ and TiO₂/rGO-320 hybrids demonstrate type IV isotherm with a H3-type hysteresis loops, and the highest adsorption at the high relative pressure (*P*/*P*₀) approaches 1. Additionally, the peak located at about 50 to 80 nm from the pore distribution curve (inset in Fig. 3) demonstrates the presence of macropores which are originated from connection of adjacent particles (Li et al., 2015a), which could also be observed from TEM images. The specific surface area of TiO₂/rGO-320 is slightly decreased with compared to the pure TiO₂. This might be caused by the long time calcinations in air. The as obtained CQDs and rGO sheet are expected to improve the penetration and adsorption of pollutants and to allow quick transport of reaction species onto the active sites.

Optical Properties

Fig. 4A shows the UV-Vis absorption spectroscopy of pure TiO₂ and TiO₂/rGO-320. The absorption edge of the hybrid does not change. In addition, the enhanced UV light absorption shows a flat but evident absorption over the test

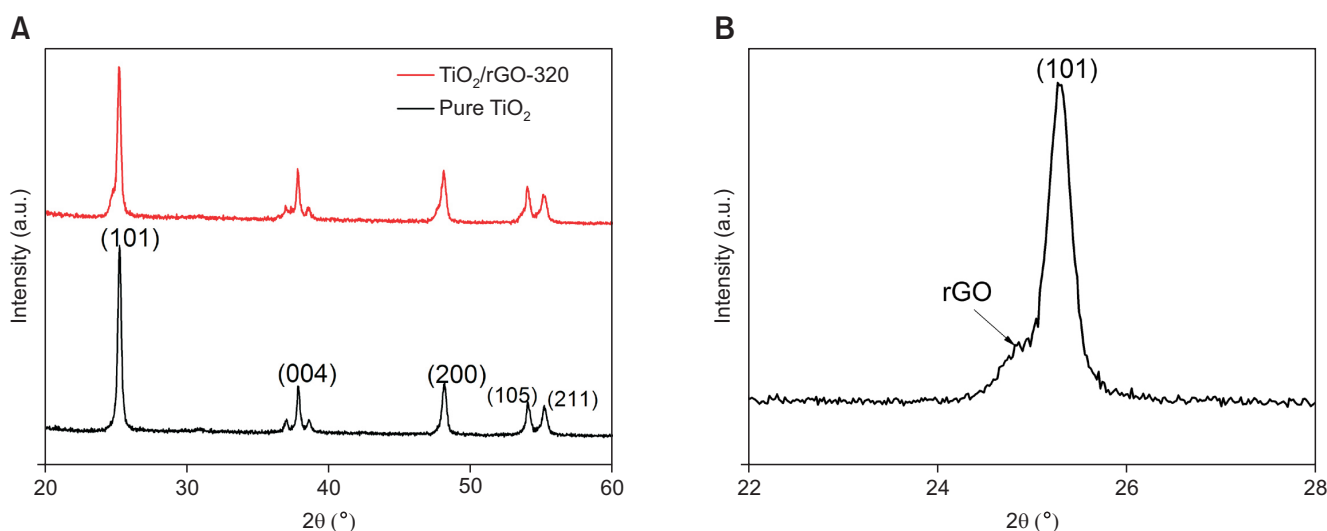


Fig. 1. X-ray diffraction patterns of TiO₂ and TiO₂/rGO-320 (A) and local magnification of TiO₂/rGO-320 (B). rGO, reduced graphene oxide.

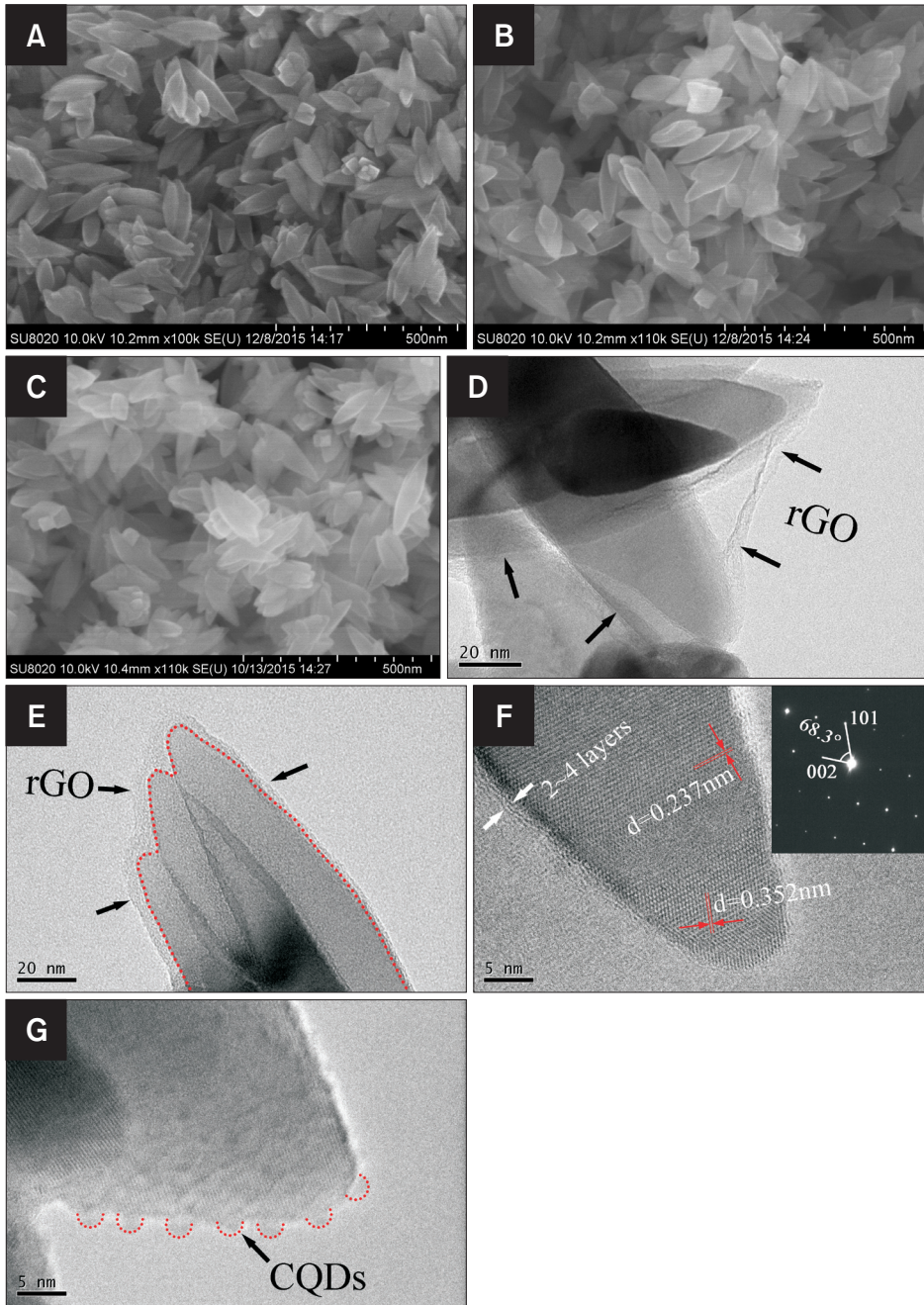


Fig. 2. Scanning electron microscope images of TiO_2/rGO (A), $\text{TiO}_2/\text{rGO-320}$ (B), and pure TiO_2 (C). Transmission electron microscopy images of TiO_2/rGO after solvothermal process (D-F) and $\text{TiO}_2/\text{rGO-320}$ (G). rGO, reduced graphene oxide; CQDs, carbon quantum dots.

range of wavelengths, which demonstrates the hybrid may be able to absorb more light and thus favor the catalysis. Fig. 4B shows FTIR spectra of $\text{TiO}_2/\text{rGO-320}$ and GO. Peak located at $1,737\text{ cm}^{-1}$ can be assigned to C=O stretching of the residual COOH groups (Thakur & Karak, 2012), $1,051\text{ cm}^{-1}$ for C-O stretching, $1,207\text{ cm}^{-1}$ for C-O-C stretching. The almost disappeared C=O bond and these relative weakened C-O/C-O-C indicate the partially reduction of GO. The broad infrared (IR) band at $500\text{ to }900\text{ cm}^{-1}$ corresponds to the Ti-O-Ti stretching vibration modes in crystalline TiO_2 and peak

at 799 cm^{-1} is assigned to Ti-O-C bond (Jiang et al., 2011; Zhang et al., 2009). These broad IR bands with high intensity demonstrate the strongly chemical interaction between rGO and TiO_2 . The peak at $1,609\text{ cm}^{-1}$ originates from skeletal vibrations of graphitic domains (Li et al., 2015b).

XPS analysis is employed to identify the surface structure information. The chemical states of Ti atoms in $\text{TiO}_2/\text{rGO-320}$ were studied through the Ti 2p XPS spectra in Fig. 5A. Two main peaks located at 458.5 eV and 464.1 eV are assigned to the Ti (2p $3/2$) and Ti (2p $1/3$) in the Ti^{4+} oxidation state (Ma

et al., 2010; Yu et al., 2013). The O1s spectra is demonstrated in Fig. 5B. The peak at 530.6 eV can be assigned to hydroxyl groups which comes from the physically or chemically adsorbed water on TiO₂ surface, and the peak at 529.7 eV corresponds to lattice oxygen in TiO₂ (Tu et al., 2013). There are five peaks in the C1s spectra, where the highest peak of C-C bond at 284.8 eV and C=C at 283.6 eV are originated from the graphitic sp² carbon atoms, which represents the excellent restoration of the sp²-hybridized carbon by the solvothermal reduction procedure (Xiu et al., 2015; Xu et al., 2010; Zhang et al., 2011). C-O-C bond at 286.3 eV and C=O bond (carboxylate impurities) at 288.7 eV are rather low demonstrating the removal of most oxygen-containing functional groups (Dey et al., 2012; Paredes et al., 2009; Tu et

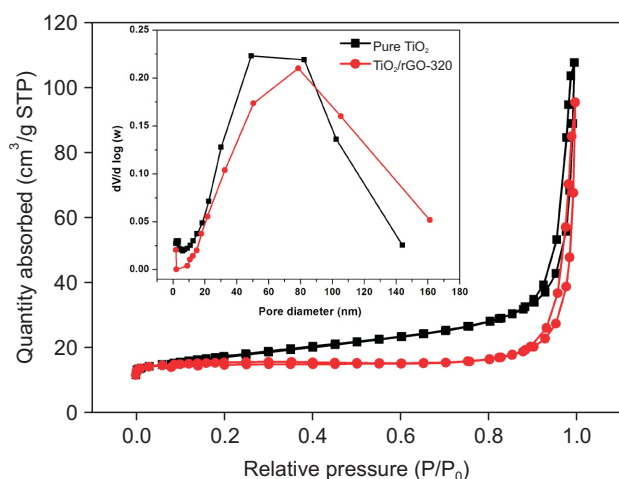
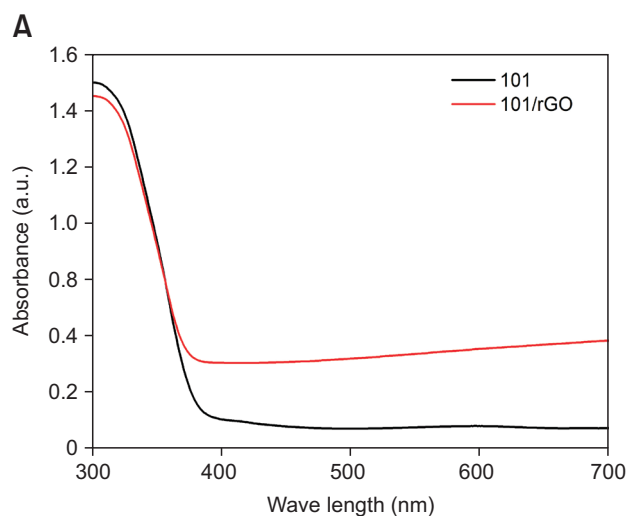


Fig. 3. N₂ adsorption-desorption N₂ adsorption-desorption isotherms. Inset is the poresize distribution. rGO, reduced graphene oxide; STP, standard temperature and pressure.



al., 2013). Peak at 288.1 eV can be ascribed to Ti-O-C bond which agrees well with the FTIR results (Qiu et al., 2015; Zhang & Pan, 2011).

Photocatalytic Activities

The photocatalytic activities of the samples were evaluated by degradation of MO under UV light irradiation. Fig. 6A shows the time profiles of (C/C₀), where C₀ represents the concentration at the adsorption-desorption equilibrium of the photocatalyst before illumination and C is the concentration at the illumination time. Compared to P25, the kinetic constants of pure TiO₂ and TiO₂/rGO-320 for degradation of MO increase by almost 2.3 and 7.7 times, respectively. TiO₂/rGO-320 shows the highest degradation efficiency (k=0.7898), about 3.3 times higher than pure TiO₂. We attribute this high photocatalytic activity to the following three points: i) enhanced electron-hole pairs separation, matching and overlapping of d-orbital of TiO₂ and π-orbital of graphene in energy levels to form d-π electron orbital (Jiang et al., 2011). Additionally, PEI polymerize and form direct chemical bonding interactions, thus the electron excited from TiO₂ under UV light can be shuttled freely into graphene network, accelerating electron transport and inhibiting e-h recombination. As TiO₂ shows a characteristic of single

Table 1. Physical parameters of BET specific surface area, pore diameter, pore volume of TiO₂ and TiO₂/rGO-320

Sample	S _{BET} (m ² /g)	Pore size (nm)	Pore volume (cm ³ /g)
P25	50	19	0.21
Pure TiO ₂	33	18	0.16
TiO ₂ /rGO-320	22	25	0.14

BET, Brunauer-Emmet-Teller; rGO, reduced graphene oxide.

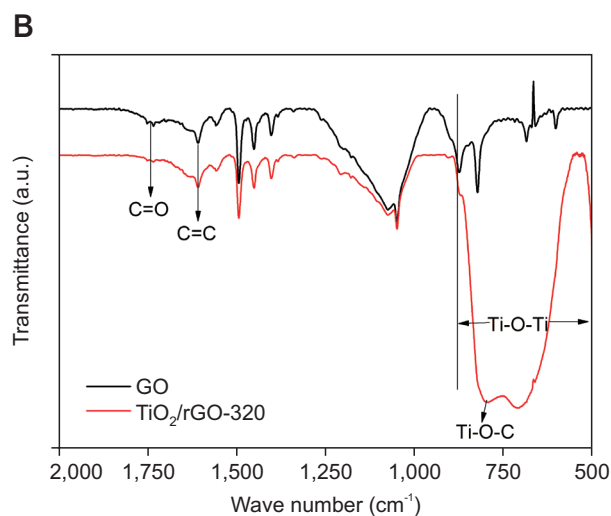


Fig. 4. UV-Vis spectra of TiO₂ and TiO₂/rGO-320 (A) and Fourier transform infrared spectra of GO and TiO₂/rGO-320 (B). rGO, reduced graphene oxide; GO, graphene oxide.

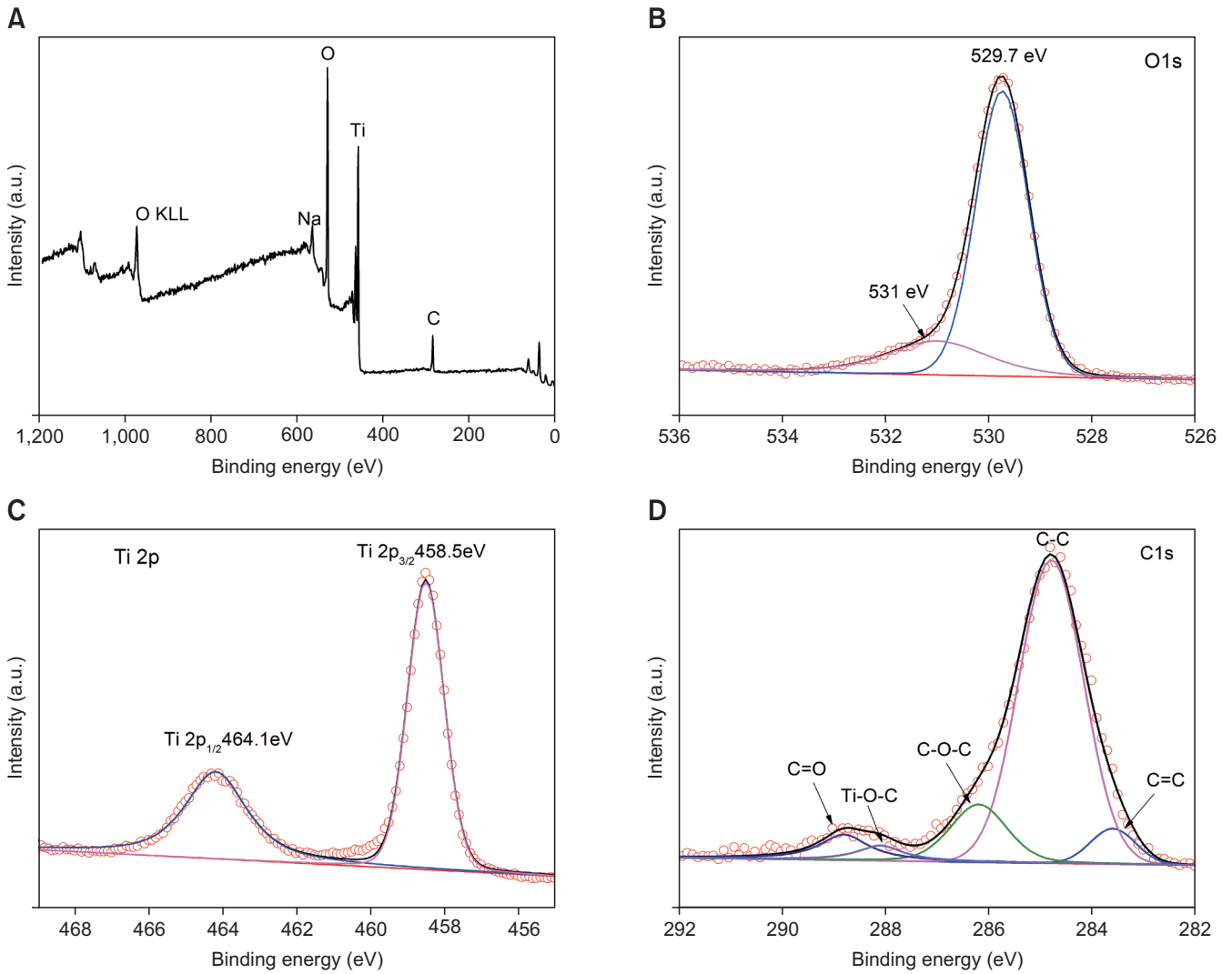


Fig. 5. (A) X-ray photoelectron spectra (XPS) wide spectra and XPS spectra of O1s (B), Ti 2p (C), and C1s (D). The open circles are the raw data of the XPS spectra.

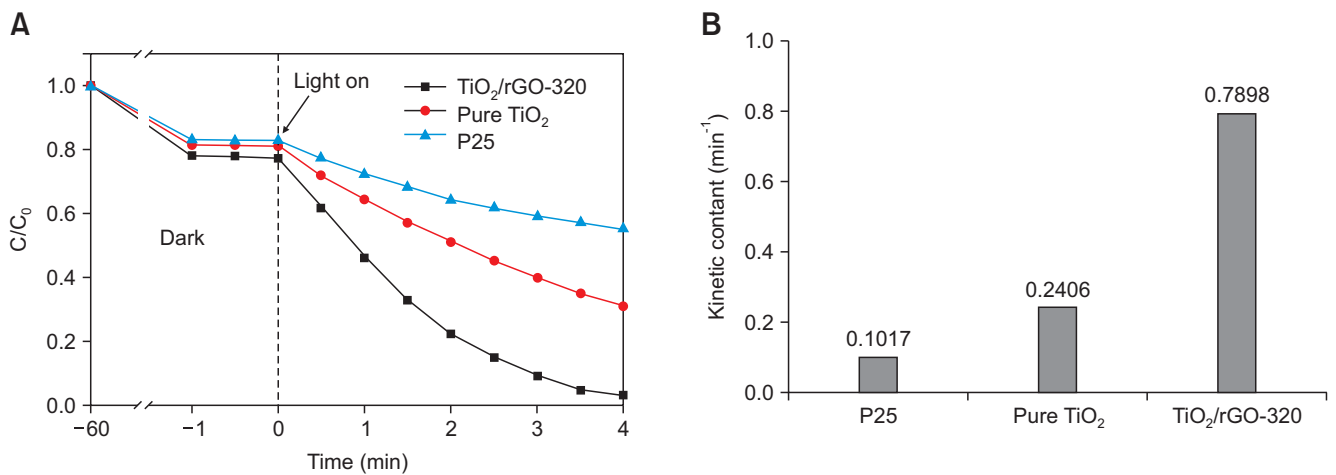


Fig. 6. Photodegradation of methyl orange under ultraviolet light irradiation (A) and kinetic constants of P25, TiO_2 , $\text{TiO}_2/\text{rGO-320}$ (B). rGO, reduced graphene oxide.

crystal, the disappearance of grain boundaries also restrict the formation of recombination centers and potential barriers (K et al., 2015). ii) Enhanced light absorption over the range of wavelengths favors photocatalysis. iii) Although TiO₂/rGO has a lower specific surface area, it shows the highest degradation rate since the reduction of GO into rGO is favorable for eliminating most oxygen-containing functional groups, leading to strong adsorption of MO on TiO₂/rGO-320 and offering more active sites for MO molecules to be oxidized.

CONCLUSIONS

Through utilizing PEI to modulate the surface charges of TiO₂ and GO, we successfully synthesize TiO₂/rGO hybrids. By an ethonal-solvothermal process, GO is reduced into rGO and most oxygen-containing functional groups are removed.

Especially, TiO₂ wrapped by graphene and CQDs is produced, resulting larger contact area and active sites after heat treatment in air. The hybrid shows excellent photocatalytic performance with a higher degradation rate about 3.3 and 7.7 times compared to the pure anatase TiO₂ bipyramids and P25, respectively. In this system, rGO and CQDs serve as an acceptor of the photogenerated electrons and minimize charge recombination rate, and enable more electrons transfer to TiO₂ surface and react with MO.

CONFLICT OF INTEREST

No potential conflict of interest relevant to this article was reported.

REFERENCES

- Allen M J, Tung V C, and Kaner R B (2009) Honeycomb carbon: a review of graphene. *Chem. Rev.* **110**, 132-145.
- Cao A, Liu Z, Chu S, Wu M, Ye Z, Cai Z, Chang Y L, Wang S F, Gong Q H, and Liu Y F (2010) A facile one-step method to produce graphene-CdS quantum dot nanocomposites as promising optoelectronic materials. *Adv. Mater.* **22**, 103-106.
- Cargnello M, Gordon T R, and Murray C B (2014) Solution-phase synthesis of titanium dioxide nanoparticles and nanocrystals. *Chem. Rev.* **114**, 9319-9345.
- Chen H, Nanayakkara C E, and Grassian V H (2012) Titanium dioxide photocatalysis in atmospheric chemistry. *Chem. Rev.* **112**, 5919-5948.
- Dey R S, Hajra S, Sahu R K, Raj C R, and Panigrahi M K (2012) A rapid room temperature chemical route for the synthesis of graphene: metal-mediated reduction of graphene oxide. *Chem. Commun.* **48**, 1787-1789.
- Fattakhova-Rohlfing D, Zaleska A, and Bein T (2014) Three-dimensional titanium dioxide nanomaterials. *Chem. Rev.* **114**, 9487-9558.
- Jiang B J, Tian C G, Zhou W, Wang J Q, Xie Y, Pan Q J, Ren Z Y, Dong Y Z, Fu D, Han J L, and Fu H G (2011) In situ growth of TiO₂ in interlayers of expanded graphite for the fabrication of TiO₂-graphene with enhanced photocatalytic activity. *Chem. Eur. J.* **17**, 8379-8387.
- K A J, Naduvath J, Mallick S, Shripathi T, Thankamoniamma M, and Philip R R (2015) A novel cost effective fabrication technique for highly preferential oriented TiO₂ nanotubes. *Nanoscale* **7**, 20386-20390.
- Kim H I, Moon G H, Monllor-Satoca D, Park Y, and Choi W Y (2012) Solar photoconversion using graphene/TiO₂ composites: nanographene shell on TiO₂ core versus TiO₂ nanoparticles on graphene sheet. *J. Phys. Chem. C* **116**, 1535-1543.
- Li Q, Guo B D, Yu J G, Ran J G, Zhang B H, Yan H J, and Gong J R (2011) Highly efficient visible-light-driven photocatalytic hydrogen production of CdS-cluster-decorated graphene nanosheets. *J. Am. Chem. Soc.* **133**, 10878-10884.
- Li W, Wang F, Feng S H, Wang J X, Sun Z K, Li B, Li Y H, Yang J P, Elzatahry A A, Xia Y Y, and Zhao D Y (2013) Sol-gel design strategy for ultradispersed TiO₂ nanoparticles on graphene for high-performance lithium ion batteries. *J. Am. Chem. Soc.* **135**, 18300-18303.
- Li W, Wang F, Liu Y P, Wang J X, Yang J P, Zhang L J, Elzatahry A A, Al-Enizi A M, Xia Y Y, and Zhao D Y (2015b) General strategy to synthesize uniform mesoporous TiO₂/graphene/mesoporous TiO₂ sandwich-like nanosheets for highly reversible lithium storage. *Nano Lett.* **15**, 2186-2193.
- Li Y L, Wang J S, Yang Y L, Zhang Y, He D, An Q E, and Cao G Z (2015a) Seed-induced growing various TiO₂ nanostructures on g-C₃N₄ nanosheets with much enhanced photocatalytic activity under visible light. *J. Hazard. Mater.* **292**, 79-89.
- Liu Y, Che R C, Chen G, Fan J W, Sun Z K, Wu Z X, Wang M H, Li B, Wei J, Wei Y, Wang G, Guan G Z, Elzatahry A A, Bagabas A A, Al-Enizi A M, Deng Y H, Peng H S, and Zhao D Y (2015) Radially oriented mesoporous TiO₂ microspheres with single-crystal-like anatase walls for high-efficiency optoelectronic devices. *Sci. Adv.* **1**, e1500166.
- Ma J, Qiang L, Tang X, and Li H (2010) A simple and rapid method to directly synthesize TiO₂/SBA-16 with different TiO₂ loading and its photocatalytic degradation performance on rhodamine B. *Catal. Lett.* **138**, 88-95.
- Paredes J I, Villar-Rodil S, Solís-Fernández P, Martínez-Alonso A, and Tascón J M D (2009) Atomic force and scanning tunneling microscopy imaging of graphene nanosheets derived from graphite oxide. *Langmuir* **25**, 5957-5968.
- Qiu B C, Zhou Y, Ma Y F, Yang X L, Sheng W Q, Xing M Y, and Zhang J L (2015) Facile synthesis of the Ti³⁺ self-doped TiO₂-graphene nanosheet composites with enhanced photocatalysis. *Sci. Rep.* **5**, 1-6.
- Tang Z H, Shen S L, Zhuang J, and Wang X (2010) Noble-metal-promoted three-dimensional macroassembly of single-layered graphene oxide. *Angew. Chem. Int. Ed.* **122**, 4707-4711.
- Thakur S and Karak N (2012) Green reduction of graphene oxide by aqueous phytoextracts. *Carbon* **50**, 5331-5339.
- Tu W G, Zhou Y, Liu Q, Yan S C, Bao S S, Wang X Y, Xiao M, and Zou Z G (2013) An in situ simultaneous reduction-hydrolysis technique for

- fabrication of TiO₂-graphene 2D sandwich-like hybrid nanosheets: graphene-promoted selectivity of photocatalytic-driven hydrogenation and coupling of CO₂ into methane and ethane. *Adv. Funct. Mater.* **23**, 1743-1749.
- Wang D H, Choi D, Li J, Yang Z G, Nie Z, Kou R, Hu D H, Wang C M, Saraf L V, Zhang J G, Aksay I A, and Liu J (2009) Self-assembled TiO₂-graphene hybrid nanostructures for enhanced li-ion insertion. *ACS Nano* **3**, 907-914.
- Wang L and Sasaki T (2014) Titanium oxide nanosheets: graphene analogues with versatile functionalities. *Chem. Rev.* **114**, 9455-9486.
- Wang X D, Li Z D, Shi J, and Yu Y H (2014) One-dimensional titanium dioxide nanomaterials: nanowires, nanorods, and nanobelts. *Chem. Rev.* **114**, 9346-9384.
- Wu H B, Hng H H, and Lou X W D (2012) Direct synthesis of anatase TiO₂ nanowires with enhanced photocatalytic activity. *Adv. Mater.* **24**, 2567-2571.
- Xiu Z L, X P Hao, Wu Y Z, Lu Q F, and Liu S W (2015) Graphene-bonded and-encapsulated mesoporous TiO₂ microspheres as a high-performance anode material for lithium ion batteries. *J. Power Sources* **287**, 334-340.
- Xu Y X, Sheng K X, Li C, and Shi G Q (2010) Self-assembled graphene hydrogel via a one-step hydrothermal process. *ACS Nano* **4**, 4324-4330.
- Yang H G, Liu G, Qiao S Z, Sun C H, Jin Y G, Smith S C, Zou J, Cheng H M, and Lu G Q (2009) Solvothermal synthesis and photoreactivity of anatase TiO₂ nanosheets with dominant {001} facets. *J. Am. Chem. Soc.* **131**, 4078-4083.
- Yang H G, Sun C H, Qiao S Z, Zou J, Liu G, Smith S C, Cheng H M, and Lu G Q (2008) Anatase TiO₂ single crystals with a large percentage of reactive facets. *Nature* **453**, 638-641.
- Yu J G, Wang S H, Low J X, and Xiao W (2013) Enhanced photocatalytic performance of direct Z-scheme g-C₃N₄-TiO₂ photocatalysts for the decomposition of formaldehyde in air. *Phys. Chem. Chem. Phys.* **15**, 16883-16890.
- Zhang H, Lv X J, Li Y M, Wang Y, and Li J H (2009) P25-graphene composite as a high performance photocatalyst. *ACS nano* **4**, 380-386.
- Zhang J, Xiong Z, and Zhao X S (2011) Graphene-metal-oxide composites for the degradation of dyes under visible light irradiation. *J. Mater. Chem.* **21**, 3634-3640.
- Zhang X F, Zhang B Y, Huang D K, Yuan H L, Wang M K, and Shen Y (2014) TiO₂ nanotubes modified with electrochemically reduced graphene oxide for photoelectrochemical water splitting. *Carbon* **80**, 591-598.
- Zhang Y P and Pan C X (2011) TiO₂/graphene composite from thermal reaction of graphene oxide and its photocatalytic activity in visible light. *J. Mater. Sci.* **46**, 2622-2626.
- Zou L, Qiao Y, Wu X S, Ma C X, Lia X, and Li C M (2015) Synergistic effect of titanium dioxide nanocrystal/reduced graphene oxide hybrid on enhancement of microbial electrocatalysis. *J. Power Sources* **276**, 208-214.